

Structural, static and dynamic magnetic properties of Co₂MnGe thin films on a sapphire a-plane substrate

M. Belmeguenai¹, F. Zighem², T. Chauveau¹, D. Faurie¹, Y. Roussigné¹, S. M. Chérif¹, P. Moch¹, K. Westerholt³ and P. Monod⁴

¹ LPMTM, Institut Galilée, UPR 9001 CNRS, Université Paris 13,

99 Avenue Jean-Baptiste Clément F-93430 Villetaneuse, France

² LLB (CEA CNRS UMR 12), Centre d'études de Saclay, 91191 Gif-Sur-Yvette, France

³ Ruhr-Universität Bochum, 44780 Bochum, Germany and

⁴ LPEM, UPR A0005 CNRS, ESPCI, 10 Rue Vauquelin, F-75231 Paris cedex 5, France

Magnetic properties of Co₂MnGe thin films of different thicknesses (13, 34, 55, 83, 100 and 200 nm), grown by RF sputtering at 400 °C on single crystal sapphire substrates, were studied using vibrating sample magnetometry (VSM) and conventional or micro-strip line (MS) ferromagnetic resonance (FMR). Their behavior is described assuming a magnetic energy density showing twofold and fourfold in-plane anisotropies with some misalignment between their principal directions. For all the samples, the easy axis of the fourfold anisotropy is parallel to the **c**-axis of the substrate while the direction of the twofold anisotropy easy axis varies from sample to sample and seems to be strongly influenced by the growth conditions. Its direction is most probably monitored by the slight unavoidable angle of miscut the Al₂O₃ substrate. The twofold in-plane anisotropy field H_u is almost temperature independent, in contrast with the fourfold field H_4 which is a decreasing function of the temperature. Finally, we study the frequency dependence of the observed line-width of the resonant mode and we conclude to a typical Gilbert damping constant α value of 0.0065 for the 55-nm-thick film.

PACS numbers:

Keywords:

I. Introduction

Ferromagnetic Heusler half metals with full spin polarization at the Fermi level are considered as potential candidates for injecting a spin-polarized current from a ferromagnet into a semiconductor and for developing sensitive spintronic devices [1]. Some Heusler alloys, like Co₂MnGe, are especially promising for these applications due to their high Curie temperature (905 K) [2] and to their good lattice matching with some technologically important semiconductors [3]. Therefore, great attention was recently paid to this class of Heusler alloys [4-10].

In a previous work [11], we used conventional and micro-strip line (MS) ferromagnetic resonance (FMR), as well as Brillouin light scattering (BLS) to study magnetic properties of 34-nm-, 55-nm- and 83-nm-thick Co₂MnGe films at room temperature. We showed that the in-plane anisotropy is described by the superposition of a twofold and of a fourfold term. The easy axes of the fourfold anisotropy were found parallel to the **c**-axis of the Al₂O₃ substrate (and, consequently, the hard axes lie at $\pm 45^\circ$ of **c**). The easy axes of the twofold anisotropy were found at $\pm 45^\circ$ of **c** for the 34-nm- and 55-nm-thick films and slightly misaligned with this orientation in the case of the 83-nm-thick sample. However, a detailed study of the in-plane anisotropy, involving temperature and thickness dependence, allowing for their physical interpretation is still missing. Therefore, it forms the aim of the present paper. Rather complete X-ray diffraction (XRD) measurements over a large thickness range of Co₂MnGe films are reported below

in an attempt to find correlations between in-plane anisotropies, thickness and crystallographic textures. The thickness- and the temperature-dependence of these anisotropies are investigated using vibrating sample magnetometry (VSM) and the above mentioned FMR techniques. In addition, we present intrinsic damping parameters deduced from broadband FMR data obtained with the help of a vector network analyzer (VNA) [12-14].

I. Sample properties and preparation

Co₂MnGe films with 13, 34, 55, 83, 100 and 200 nm thickness were grown on sapphire **a**-plane substrates (showing an in-plane **c**-axis) by RF-sputtering with a final 4 nm thick gold over layer. A more detailed description of the sample preparation procedure can be found elsewhere [11, 15].

The static magnetic measurements were carried out at room temperature using a vibrating sample magnetometer (VSM). The dynamic magnetic properties were investigated with the help of 9.5 GHz conventional FMR and of MS-FMR [11]. The conventional FMR set-up consists in a bipolar X-band Bruker ESR spectrometer equipped with a TE₁₀₂ resonant cavity immersed in an Oxford cryostat, allowing for exploring the 4-300 K temperature interval. The MS-FMR set-up is home-made designed and, up to now, only works at room temperature. The resonance fields (conventional FMR) and frequencies (MS-FMR) are obtained from a fit assuming a Lorentzian derivative shape of the recorded data. The experimental results are analyzed in

the frame of the model presented in [11].

XRD experiments were performed using four circles diffractometers in Bragg-Brentano geometry in order to determine $\theta - 2\theta$ patterns and pole figures. The diffractometer devoted to the $\theta - 2\theta$ patterns was equipped with a point detector (providing a precision of 0.015° in 2θ scale). The instrument used for recording pole figures was equipped with an InelTM curved linear detector (120° aperture with a precision of 0.015° in 2θ scale). The X-rays beams (Cobalt line focussource at $\lambda = 1.78897$) were emitted by a BrukerTM rotating anode. define a direct macroscopic ortho-normal reference (**1**, **2**, **3**), where the **3**axis stands for the direction normal to the film. The $\theta - 2\theta$ patterns (not shown here) indicate that, for all the Co₂MnGe thin films, the $\langle 110 \rangle$ axis can be taken along the **3**-axis. The Co₂MnGe deduced lattice constant ($a = 5.755$ is in good agreement with the previously published ones [6, 16]. Due to the $[111]$ preferred orientation of the gold over layer along the **3**-axis, only partial $\{110\}$ pole figures could be efficiently exploited. They behave as $\{110\}$ fiber textures containing well defined zones showing significantly higher intensities (Figure 1 (a) and (b)). These regions correspond to orientation variants which can be grouped into two families (see Figure 1). The first one, where the threefold $[1\bar{1}1]$ or the $[11\bar{1}]$ axis is oriented along the **c** rhombohedral direction, consists of two kinds of distinct domains with the $[001]$ axis at $\pm 54.5^\circ$ from the **c**-axis. The second family, which is rotated around the **3**-axis by 90° from the first one, also contains two variants. This peculiar in-plane domain structure is presumably induced by the underlying vanadium seed layer. As illustrated in Figure 1c, which represents φ -scans at $\theta = 60^\circ$, we do not observe major differences between the crystallographic textures of the 55-nm and of the 100-nm-thick samples : the first family shows a concentration twice larger than the second one ; at least for the first family, which allows for quantitative evaluations, the concentrations of the two variants do not appreciably differ from each other; finally, about 50% of the total scattered intensity arises from domains belonging to these oriented parts of the scans. In the 200-nm-thick sample the anisotropy of the fiber is less marked but the two families remain present.

III. Results and discussion

1- Static magnetic measurements

In order to study the magnetic anisotropy at room temperature, the hysteresis loops were measured for all the studied films with an in-plane applied magnetic field along various orientations as shown in Figure 2 (φ_H is the in-plane angle between the magnetic applied field H and the **c**-axis of the substrate). The variations of the coercive field (H_c) and of the reduced remanent magnetization (M_r/M_s) were then investigated as function of φ_H .

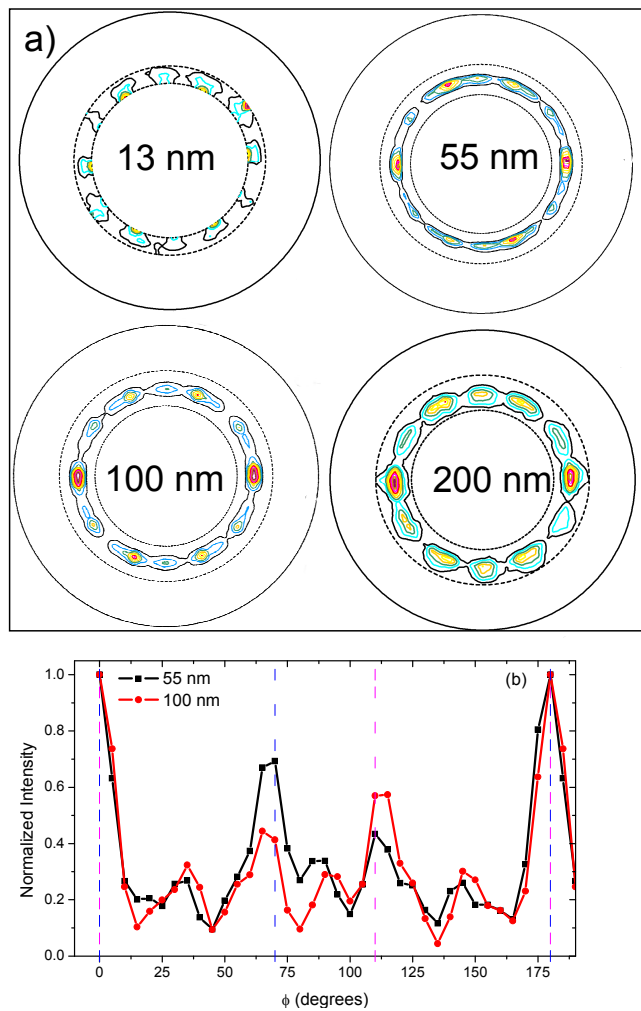


Figure 1: (Color online) (a) Partial $\{110\}$ X-rays pole figures (around 60°) of 13, 55, 100 and 200-nm-thick films. (b) Display of the angular variations of the intensity derived from the above figures for the 55 and 100-nm-thick samples (the blue and pink vertical dashed lines respectively refer to the two expected positions of the diffraction peak relative to the two variants belonging to family 1).

The typical behavior is illustrated below through two representative films which present different anisotropies.

Figure 2a shows the loops along four orientations for the 100-nm-thick sample. One observes differences in shape of the normalized hysteresis loops depending upon the field orientation. For H along **c** ($\varphi_H = 0^\circ$) we observe a typical easy axis square-shaped loop with a nearly full normalized remanence ($M_r/M_s = 0.9$), a coercive field of about 20 Oe and a saturation field of 100 Oe. As φ_H increases away from the **c** axis direction, the coercivity increases and the hysteresis loop tends to transform into a hard axis loop. When φ_H slightly overpasses 90° ($90^\circ < \varphi_H < 100^\circ$) the loop evolves into a more complicated shape: it becomes composed of three (or two) open smaller loops. Further increasing the in-plane rotation angle, it changes from such a split-open curve up to

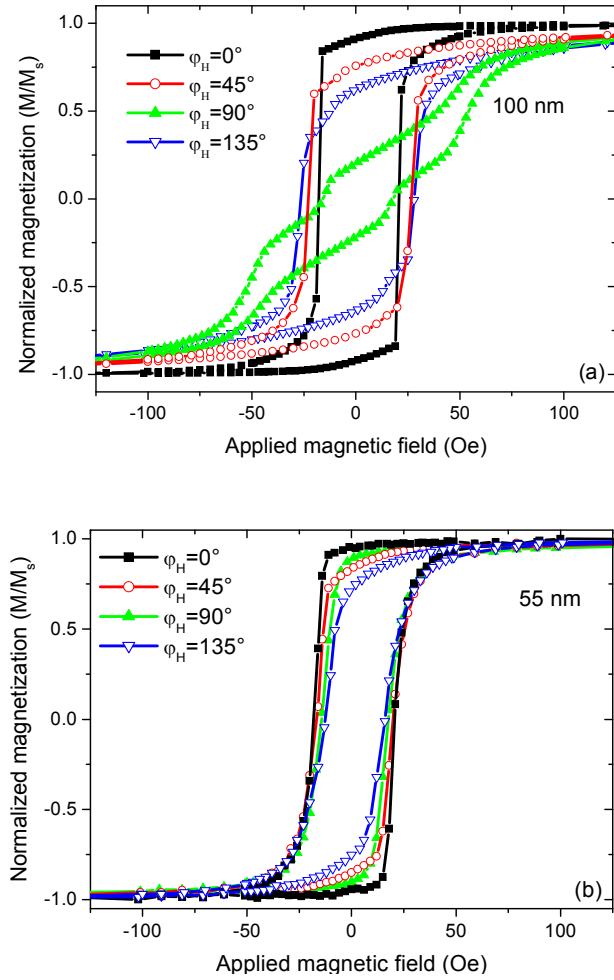


Figure 2: (Color online) VSM magnetization loops of the (a) 100-nm-thick and the (b) 55-nm-thick samples. The magnetic field is applied parallel to the film surface, at various angles (φ_H) with the c axis of the sapphire substrate.

an almost rectangular shape. The results for $\varphi_H = 45^\circ$ and $\varphi_H = 135^\circ$ are different: they show a rounded loop with M_r/M_s equal to 0.75 and 0.63 and with saturation fields are about 170 Oe and 200 Oe, respectively. This result qualitatively agrees with a description of the in-plane anisotropy in terms of four-fold and two-fold contributions with slightly misaligned easy axes.

The variations of H_c and M_r/M_s versus φ_H are illustrated in Figures 3a and 3b for the 100-nm-thick film. The presence of a fourfold anisotropy contribution is supported by the behavior of H_c (Figure 3a), since two minima appear within each period (180° , as expected), as shown in Figure 3a. The minimum minimum is mainly related to the uniaxial anisotropy term. In the same way, as displayed in Figure 3b, the behavior of M_r/M_s is dominated by the uniaxial anisotropy. It is worth to notice that the minimum minimum position slightly differs

from 90° (lying around 96°), thus arguing for a misalignment between the twofold and the fourfold anisotropy axes.

Figure 2b shows a series of hysteresis loops, recorded with an in-plane applied field, for the 55-nm-thick film. A careful examination suggests that the fourfold anisotropy contribution is the dominant one and that the related easy axis lies along c . The M_r/M_s variation versus φ_H , reported in Figure 3c, is consistent with an easy uniaxial axis oriented at 45° of this last direction. Both fourfold and uniaxial terms are smaller than for the 100-nm-thick sample.

2- Dynamic magnetic properties

As previously published [11], the dynamic properties are tentatively interpreted assuming a magnetic energy density which, in addition to Zeeman, demagnetizing and exchange terms, is characterized by the following anisotropy contribution:

$$E_{anis.} = K_{\perp} \sin^2 \theta_M - \frac{1}{2}(1 + \cos(2(\varphi_M - \varphi_u)))K_u \sin^2 \theta_M - \frac{1}{8}(3 + \cos 4(\varphi_M - \varphi_4))K_4 \sin^4 \theta_M \quad (1)$$

In the above expression, θ_M and φ_M respectively represent the out-of-plane and the in-plane (referring to the c -axis of the substrate) angles defining the direction of the magnetization M_s ; φ_u and φ_4 stand for the angles of the uniaxial axis and of the easy fourfold axis, respectively, with this c -axis. With these definitions K_u and K_4 are necessarily positive. As done in ref. [11], it is often convenient to introduce the effective magnetization $4\pi M_{eff} = 4\pi M_s - 2K/M_s$, the uniaxial in-plane anisotropy field $H_u = 2K_u/M_s$ and the fourfold in-plane anisotropy field $H_4 = 4K_4/M_s$.

For an in-plane applied magnetic field \mathbf{H} , the studied model provides the following expression for the frequencies of the experimentally observable magnetic modes:

$$F_n = \frac{\gamma}{2\pi} (H \cos(\varphi_H - \varphi_M) + \frac{2K_4}{M_s} \cos 4(\varphi_M - \varphi_4) + \frac{2K_u}{M_s} \cos 2(\varphi_M - \varphi_u) + \frac{2A_{ex}}{M_s} (\frac{n\pi}{d})^2) \times (H \cos(\varphi_H - \varphi_M) + 4\pi M_{eff} + \frac{K_4}{2M_s} (3 + \cos 4(\varphi_M - \varphi_4)) + \frac{K_u}{M_s} (1 + \cos 2(\varphi_M - \varphi_u)) + \frac{2A_{ex}}{M_s} (\frac{n\pi}{d})^2) \quad (2)$$

In the above expression γ is the gyromagnetic factor: $(\gamma/2\pi) = g \times 1.397 \times 10^6 \text{ Hz/Oe}$. The uniform mode corresponds to $n=0$. The other modes to be considered (perpendicular standing modes) are connected to integer values of n : their frequencies depend upon the exchange stiffness constant A_{ex} and upon the film thickness d . For all the films the magnetic parameters at room temperature were derived from MS-FMR measurements. The deduced g factor is equal to 2.17, as previously published [11].

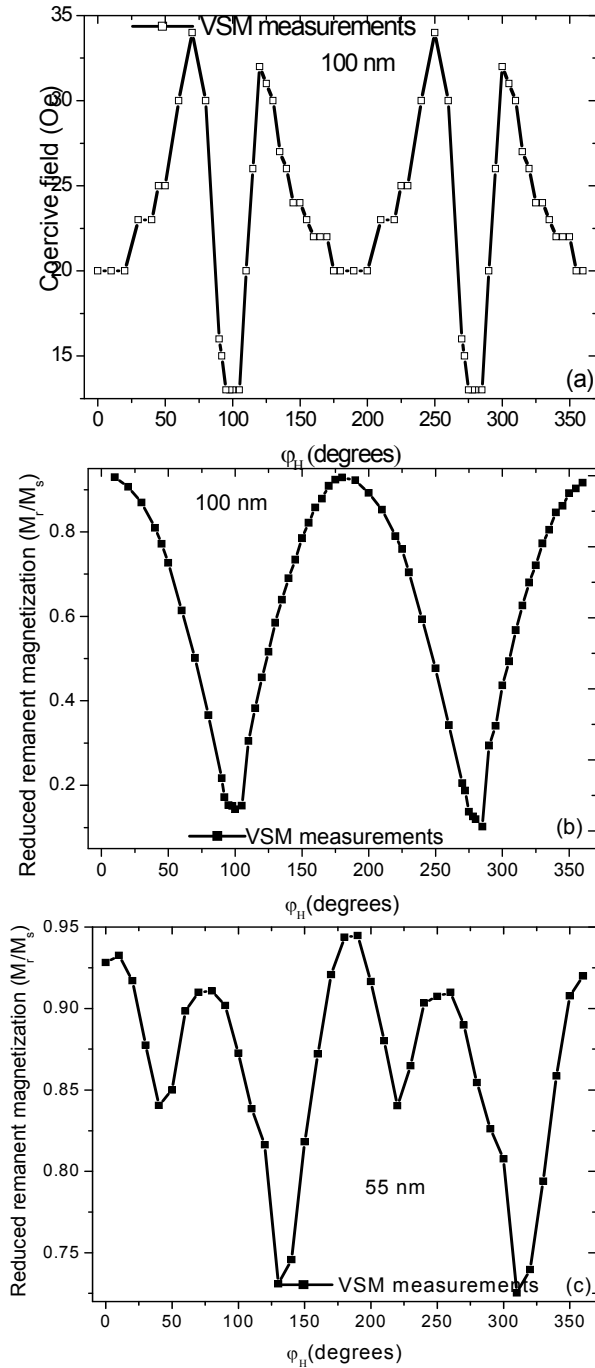


Figure 3: (a) Coercive field and (b) reduced remanent magnetization of the 100-nm-thick sample as a function of the in-plane field orientation (φ_H). (c) Reduced remanent magnetization of the 55-nm-thick-film

The in-plane MS-FMR spectrum of the 100 nm-thick sample (Figure 4a) submitted to a field of 520 Oe shows two distinct modes: a main one (mode 2), with a wide line-width (about 0.6 GHz) and a second weaker one (mode 1) at lower frequency with a narrower line-width (0.2 GHz). Their field-dependences are presented in Figure 4b. In contrast with mode 2, which presents

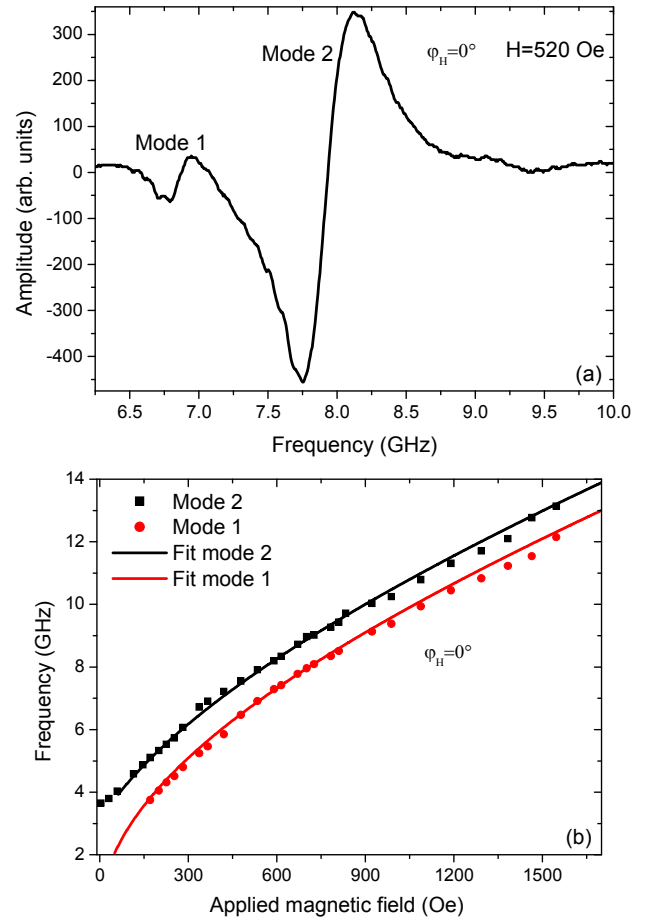


Figure 4: (Color online) (a) MS-FMR spectrum under a magnetic field applied ($H=520$ Oe) parallel the c -axis and (b) field-dependence of the resonance frequency of the uniform excited modes, in the 100-nm-thick thin film. The fits are obtained using equation (2) with the parameters indicated in Table I.

significant in-plane anisotropy, the measured resonance frequency of mode 1 does not vary versus the in-plane angular orientation of the applied magnetic field: such a different behavior prevents from attributing mode 1 to a perpendicular standing excitation. Consequently, mode 1 is presumably a uniform mode arising from the presence of an additional magnetic phase in the film, possessing a lower effective demagnetizing field. In the following, we focus on mode 2 which is assumed to be the uniform mode arising from the main phase. As previously published, only one resonance is observed with the 55-nm-thick sample.

Figures 5b and 5d illustrate the experimental in-plane angular-dependencies of the resonance frequency of the uniform mode for the 100- and for the 55-nm-thick samples, compared to the obtained fits using equation (2). As expected from the VSM measurements, in the 100-nm sample the fourfold and uniaxial axes of anisotropy are misaligned: it results an absence of symmetry of the representative graphs around $\varphi_H=$

90°. The best fit is obtained for the following values of the magnetic parameters: $4\pi M_{eff} = 9800$ Oe, $H_u = 55$ Oe, $H_4 = 110$ Oe, $\varphi_4 = 0^\circ$, $\varphi_u = 12^\circ$. As previously published, in the case of the 55-nm sample the direction of the easy uniaxial axis coincides with the observed one for the fourfold axis: this parallelism induces symmetry of the graphs around $\varphi_H = 90^\circ$. The best fit for this film corresponds to: $4\pi M_{eff} = 9800$ Oe, $H_u = 10$ Oe, $H_4 = 54$ Oe, $\varphi_4 = 0^\circ$, $\varphi_u = 45^\circ$. In both samples, the fourfold anisotropy easy direction is parallel to the \mathbf{c} axis of the substrate: this presumably results from an averaging effect of the above described distribution of the crystallographic orientations, in spite of the facts that such a conclusion requires equal concentrations of the two main variants, a condition which, strictly speaking, is not fully realized, and that the observed value of φ_4 does not derive from an apparently oversimplified averaging model that we attempted to use, based on individual domain contributions showing their principal axis of anisotropy along their cubic direction.

As usual, attempts to interpret the in-plane hysteresis loops using the coherent rotation model do not provide a quantitative evaluation of the anisotropy terms involved in the expression of magnetic energy density. However, the experimentally measured M_r/M_s angular variation, which, with this model, is given by $\cos(\varphi_M - \varphi_H)$ in zero-applied field and is easily calculated knowing φ_u , φ_4 and H_u/H_4 , is in agreement with the values of these coefficients fitted from resonance data, as shown in Figures 5a and 5c.

t (nm)	$4\pi M_{eff}$ (kG)	H_u (Oe)	H_4 (Oe)	φ_u (deg.)	φ_4 (deg.)
13	8000	45	40	12	0
34	9000	6	20	45	0
55	9800	10	54	45	0
89	9200	15	22	-5	0
100	9800	60	110	12	0
200	9900		24		0

Table I : Magnetic parameters obtained from the best fits to our experimental results. φ_u and φ_4 are the angles of in-plane uniaxial and of fourfold anisotropy easy axes, respectively

The magnetic parameters deduced from our resonance measurements are given in Table I for the complete set of the studied films. In contrast with the direction of the fourfold axis which does not vary, the orientation of the uniaxial axis is sample dependent: for some of them (34 and 55nm) the easy uniaxial direction lies at 45° from the \mathbf{c} axis of the substrate (thus coinciding with the hard fourfold direction); for other ones (13, 83, 100 nm) it shows a variable misalignment; finally, the anisotropy field vanishes for the thickest sample (200 nm). We tentatively attribute at least a fraction of the uniaxial

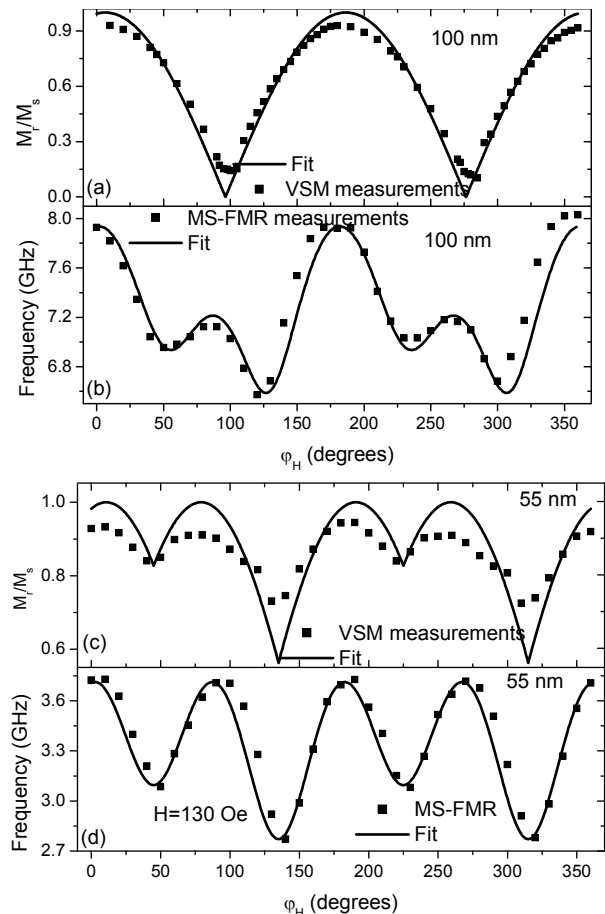


Figure 5: Reduced remanent magnetization of the (a) 100-nm- and of the (c) 55-nm-thick films. The simulations are obtained from the energy minimization using the parameters reported in Table I. (b) and (d) show the compared in-plane angular dependences of the resonance frequency of the uniform modes. The fit is obtained using equation (2) with the parameters indicated in Table I.

contribution as originating from a slight misorientation of the surface of the substrate. The amplitudes of both in-plane anisotropies are sample dependent and cannot be simply related to the film thickness. It should be mentioned that some authors [17] have reported on strain-dependent uniaxial and fourfold anisotropies in Co_2MnGa . This suggests a forthcoming experimental X-rays study of the strains present in our films.

In addition, it is useful to get information about the damping terms involved in the dynamics of magnetic excitations in the above samples. Notice that in order to integrate these films in application devices like, for instance, MRAM, it is important to make sure that their damping constant is small enough. The damping of the 55-nm-thick film was studied by VNA-FMR [12-14]: it is analyzed in terms of a Gilbert coefficient α in the Landau-Lifschitz-Gilbert equation of motion. The frequency line-

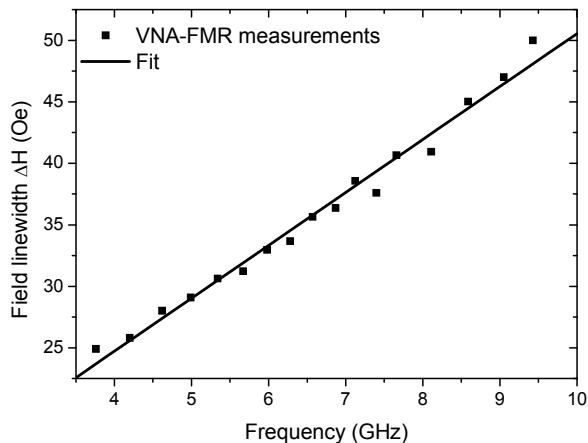


Figure 6: Line-width ΔH as a function of the resonance frequency for 55-nm-thick film. ΔH is derived from the experimental VNA-FMR frequency-swept line-width.

width Δf of the resonant signal around f_r observed using this technique is related to the field line-width ΔH measured with conventional FMR excited with a radio-frequency equal to f_r through the equation [18]:

$$\Delta H = \Delta \frac{\partial H(f)}{\partial f} \Big|_{f=f_r} \quad (3)$$

ΔH is given by:

$$\Delta H = \Delta H_0 + \frac{4\pi f_r}{|\gamma|} \alpha \quad (4)$$

(where ΔH_0 stands for a small contribution arising from inhomogeneous broadening). The measured linear dependence of ΔH shown in Figure 6. We then obtain the damping coefficient: $\alpha = 0.0065$. This value lies in the range observed in the Co_2MnSi thin films [19-21].

Finally, the temperature dependence was studied for the 55-nm-thick sample using conventional FMR. The fits of the magnetic parameters were performed assuming that g practically does not vary versus the temperature T , as generally expected. We then take: $g = 2.17$. The results for the uniaxial and for the fourfold in-plane anisotropy fields are reported in Figure 7. H_u is temperature independent while H_4 is a significantly decreasing function of T . This behavior of H_4 is presumably related to the magneto-crystalline origin of this anisotropy term.

V Summary

The static and dynamic magnetic properties of Co_2MnGe films of various thicknesses sputtered on \mathbf{a} -plane sapphire substrate have been studied. The present work focused on the dependence of the parameters describing the magnetic anisotropy upon the

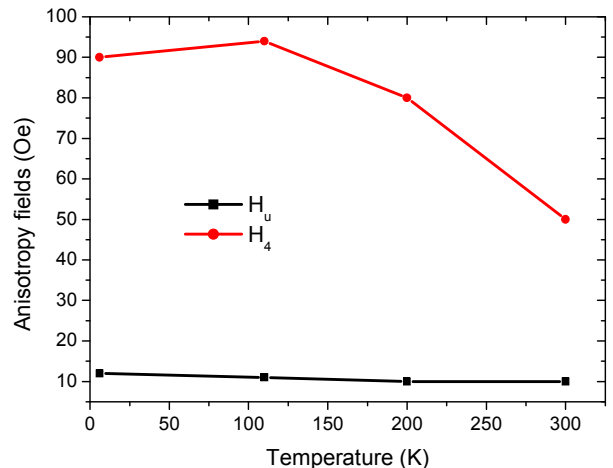


Figure 7: (Color on line) Temperature-dependence of the fourfold anisotropy field (H_4) and the uniaxial anisotropy field (H_u) of the 55-nm-thick film, measured by FMR at 9.5 GHz.

crystallographic texture and upon the thickness of the films. The crystallographic characteristics were obtained through X-ray diffraction which reveals the presence of a majority of two distinct (110) domains. Magnetometric measurements were performed by VSM and magnetization dynamics was analyzed using conventional and micro-strip resonances (FMR and MS-FMR). The main results concern the in-plane anisotropy which contributes to the magnetic energy density through two terms: a uniaxial one and fourfold one. The hard axis related to the fourfold term is always parallel to the \mathbf{c} -axis of the substrate while, depending on the sample, the easy two-fold axis coincides with \mathbf{c} or shows a variable misalignment. The fourfold anisotropy is a decreasing function of the temperature: it is presumably of magneto-crystalline nature and its orientation is related to the above noticed domains. The observed misalignment of the two-fold axis is tentatively interpreted as induced by random slight miscuts affecting the orientation of the surface of the substrate. The two-fold anisotropy does not significantly depend on the temperature. There is no evidence of a well-defined dependence of the anisotropy versus the thickness of the films. Finally, we show that the damping of the magnetization dynamics can be interpreted as arising from a Gilbert term in the equation of motion, that we evaluate.

References

- [1] S. Tsunegi, Y. Sakuraba, M. Oogane, K. Takanashi, Y. Ando, Appl. Phys. Lett. 93, 112506 (2008)
- [2] S. Picozzi, A. Continenza, and A. J. Freeman, Phys. Rev. B 66, 094421 (2002).
- [3] S. Picozzi, A. Continenza, and A. J. Freeman, J. Phys. Chem. Solids 64, 1697 (2003).
- [4] T. Ambrose, J. J. Krebs, and G. A. Prinz, J. Appl. Phys. 89, 7522 (2001).

- [5] T. Ishikawa, T. Marukame, K. Matsuda, T. Uemura, M. Arita, and M. Yamamoto, *J. Appl. Phys.* 99, 08J110 (2006)
- [6] F. Y. Yang, C. H. Shang, C. L. Chien, T. Ambrose, J. J. Krebs, G. A. Prinz, V. I. Nikitenko, V. S. Gornakov, A. J. Shapiro, and R. D. Shull, *Phys. Rev. B* 65, 174410 (2002).
- [7] H. Wang, A. Sato, K. Saito, S. Mitani, K. Takanashi, and K. Yakushiji, *Appl. Phys. Lett.* 90, 142510 (2007)
- [8] Y. Sakuraba, M. Hattori, M. Oogane, Y. Ando, H. Kato, A. Sakuma, T. Miyazaki, and H. Kubota, *Appl. Phys. Lett.* 88, 192508 (2006).
- [9] T. Marukame, T. Ishikawa, K. Matsuda, T. Uemura, and M. Yamamoto, *Appl. Phys. Lett.* 88, 262503 (2006).
- [10] D. Ebke, J. Schmalhorst, N.-N. Liu, A. Thomas, G. Reiss, and A. Hütten, *Appl. Phys. Lett.* 89, 162506 (2006).
- [11] M. Belmeguenai, F. Zighem, Y. Roussigné, S-M. Chérif, P. Moch, K. Westerholt, G. Woltersdorf, and G. Bayreuther *Phys. Rev. B* 79, 024419 (2009).
- [12] M. Belmeguenai, T. Martin, G. Woltersdorf, M. Maier, and G. Bayreuther, *Phys. Rev. B* 76, 104414 (2007).
- [13] T. Martin, M. Belmeguenai, M. Maier, K. Perzlmaier, and G. Bayreuther, *J Appl. Phys.* 101, 09C101 (2007)
- [14] M. Belmeguenai, T. Martin, G. Woltersdorf, G. Bayreuther, V. Baltz, A. K; Suszka and B. J. Hickey, *J. Phys.: Condens. Matter* 20, 345206 (2008).
- [15] U. Geiersbach, K. Westerholt and H. Back *J. Magn. Magn. Mater.* 240, 546 (2002).
- [16] T. Ambrose, J. J. Krebs, and G. A. Prinz, *J. Appl. Phys.* 87, 5463 (2000)
- [17] M. J. Pechana, C. Yua, D. Carrb, C. J. Palmstrøm, *J. Mag. Mag. Mat.* 286, 340 (2005)
- [18] S. S. Kalarickal, P. Krivosik, M. Wu, C. E. Patton, M. L. Schneider, P. Kabos, T. J. Silva, and J. P. Nibarger, *J. Appl. Phys.* 99, 093909 (2006)
- [19] R. Yilgin, M. Oogane, Y. Ando, T. Miyazaki, *J. Mag. Mag. Mat.* 310, 2322 (2007)
- [20] R. Yilgin, Y. Sakuraba, M. Oogane, S. Mizumaki, Y. Ando, and T. Miyazaki, *Japan. J. Appl. Phys.* 46, L205 (2007)
- [21] S. Trudel, O. Gaier, J. Hamrle, and B. Hillebrands, *J. Phys. D: Appl. Phys.* 43, 193001 (2010)